# Aeroelastic Optimization of Variable Stiffness Composite Wing with Blending Constraints

Bordogna, Marco Tito; Macquart, Terence; Bettebghor, D.; De Breuker, Roeland

**DOI**
10.2514/6.2016-4122

**Publication date**
2016

**Document Version**
Accepted author manuscript

**Published in**
17th AIAA/ISSMO Multidisciplinary Analysis and Optimization Conference

# Aeroelastic Optimization of Variable Stiffness Composite Wing with Blending Constraints

Marco Tito Bordogna[1 3] *Terence Macquart[2] †Dimitri Bettebghor[1] ‡
and Roeland De Breuker[3] §

[1] *ONERA - The French Aerospace Lab F-92260, Chatillon, France*
[2] *University of Bristol, Bristol, England BS8 1TR, United Kingdom*
[3] *Delft University of Technology, 2629 HS Delft, The Netherlands*

**Abstract**

Optimizing the laminates of large composite structures is nowadays well-recognized as having significant benefits in the design of lightweight structural solutions. However, designs based on locally optimized laminates are prone to structural discontinuities and enforcing blending during the optimization is therefore crucial in order to achieve structurally continuous and ready-to-manufacture designs. Bi-step strategies, relying on a continuous gradient-based optimization of lamination parameters followed by a discrete stacking sequence optimization step during which blending is enforced, have been proposed in the literature. However, significant mismatch between continuous and discrete solutions were observed due to the discrepancies between both design spaces. The present paper highlights the capability of the continuous blending constraints, recently proposed by the authors, in reducing the discrepancies between discrete and continuous solutions. The paper also demonstrates that more realistic optimal continuous designs are achieved thanks to the application of the blending constraints during the aeroelastic optimization of a variable stiffness wing. Additionally, the proposed blending constraints have been applied to NASTRAN SOL 200 showing their ease of implementation in commercial software.

## 1 Introduction

The use of composite materials in the aerospace industry is increasing steadily due to the high stiffness and strength to weight ratios of carbon fiber reinforced polymers (CFRP) with respect to their more conventional aluminium counterparts, making them ideal for lightweight structure design. Another distinctive characteristic of composites, as opposed to metals, is the possibility to adjust their anisotropic behavior by changing the stacking sequence of laminates. By doing so, composite materials allow structural designers to specifically tailor structures according to the loads they are predicted to experience. Commonly employed in the literature, the improved stiffness design of a large composite structure is obtained by dividing it into sub-structures or sections each optimized

*Ph.D. Candidate, Faculty of Aerospace Engineering, Aerospace Structures and Computational Mechanics, TU Delft
†Research Associate, Advanced Composite Center for Innovation and Science, Department of Aerospace Engineering, University of Bristol
‡Research Scientist, Département Aéroélasticité et Dynamique des Structures (DADS), ONERA
§Assistant Professor, Faculty of Aerospace Engineering, Aerospace Structures and Computational Mechanics, TU Delft

with respect to their laminate thickness and stacking sequence. However, this practice reduce the integrity of the structure due to thickness and/or stacking sequence discontinuities and do not provide any guarantee that the optimized structure could be manufactured [**?**, **?**]. In order to avoid stress concentrations due to structural discontinuities and to improve manufacturability, blending has to be taken into account throughout the design process in order to ensure ply continuity over the whole structure.

Ply continuity between structural sections can be imposed in different ways. Inner and outer blending have been introduced by Adams et al. [**?**] , in these definitions only the innermost and the outermost plies can be dropped as shown in Figure 1a. Two alternative definitions, the generalized and relaxed generalized blending, have been formulated by Van Campen et al. [**?**] and are presented in Figure 1b. Generalized blending requires all plies of the thinnest section to be continuous in the whole structure; relaxed generalized blending demands that no discontinuous plies should be in direct physical contact with each other. Throughout this paper, blending is always associated to the generalized blending definition of Van Campen et al. [**?**] for sake of clarity.

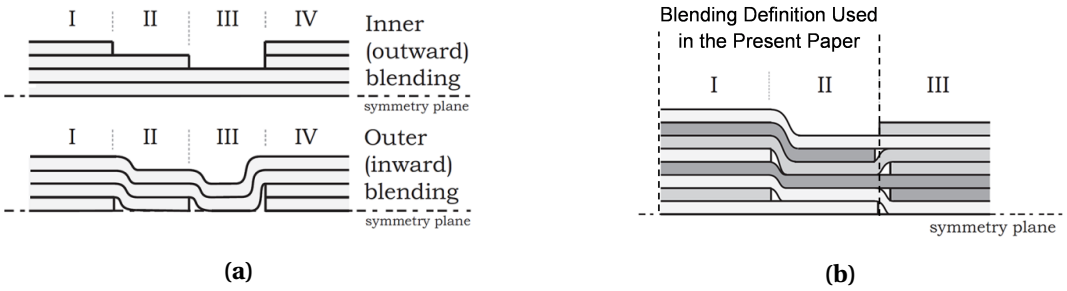


**Figure 1:** (a) Outward and inward blending, and (b) generalized (I and II) and relaxed generalized (II and III) blending. Original figures from [**?**] .

Single and multi-step optimizations have been proposed to optimize variable stiffness blended composite structures. Single step methods are usually based on heuristic techniques (e.g. genetic algorithms [**?**, **?**]) to generate populations of blended solutions. These methods are highly constrained and have prohibitive computational cost when applied to large scale optimization problems. Multi-step approaches divide the optimization into simpler-to-solve sub-optimization problems. Several authors [**?**, **?**, **?**, **?**] have used bi-step strategies where a gradient-based (continuous) optimization of homogenized stiffness parameters (e.g. lamination parameters) is followed by a genetic algorithm (discrete optimization) to retrieve blended stacking sequences. By doing so, mechanical constraints (e.g. stresses and/or buckling) are verified during the continuous step whereas most of the manufacturing constraints (e.g. blending) are enforced during the discrete step. This bi-step approach can result in significant discrepancies between the two optimization steps [**?**] and therefore there is no guarantee to find an equivalent of the optimal continuous design after the discrete step. The only viable way to satisfy both mechanical and manufacturing constraints when employing the bi-step approach is to couple the genetic algorithm used for stacking sequence retrieval with expensive mechanical constraint evaluations that can be either surrogate-model based or derived via finite element calculations.

In view of discontinuities and issues arising due to the bi-step optimization approach, Macquart

et al. [**?**] proposed employing lamination parameters combined with a set of blending constraints to be used in the continuous optimization in order to achieve more realistic and manufacturable continuous designs and reduce discrepancies between the two steps. In [**?**] the continuous blending constraints have been applied to the benchmark case of the 18 panel horseshoe [**?**] that has proven their effectiveness. The derived constraints allowed the continuous optimization to retrieve a more realistic continuous optimal design and reduced the lamination parameter space in the continuous optimization so that the continuous optimal design lays close to the discrete one retrieved with the genetic algorithm. In a continuing effort, Macquart et al. [**?**] have also demonstrated that the application of blending constraints during aeroelastic optimizations results in more realistic continuous design. Although it was shown that closely matching aeroelastic performance could be achieved during stacking sequence retrieval, these results are obtained from an in-house code based on Timoshenko beam structural model. By contrast, the present paper aims at carrying an investigation more representative of the wing design process by including local buckling constraints and a wing shell model to be optimized by the NASTRAN commercial finite element software.

This paper is organized as follow. Section 2 briefly introduces the blending constraints. The optimization strategy, the wing model and the genetic algorithm used in the discrete step are presented in Section 3. Finally, Sections 4 and 5 present the results and draw conclusions on the advantages related to using blending constraints during the aeroelastic optimization of the variable stiffness composite wing.

## 2 Blending Constraints

Lamination parameters have been first introduced by Tsai et al. [**?**] and are used to describe the stiffness matrix of composite laminates in a continuous space. For stacking sequence with discrete plies of constant thickness ($t_{ply}$) and ply angle ($\theta_i$), lamination parameters are defined in Eqs. (1). In this paper only symmetric stacking sequence with even number of ply and same thickness are considered, therefore only lamination parameters for membrane ($A$) and bending ($D$) stiffness matrices are taken into account.

$$\begin{aligned}(V_1^A, V_2^A, V_3^A, V_4^A) &= \frac{1}{N}\sum_{i=1}^{N}[\cos(2\theta_i), \sin(2\theta_i), \cos(4\theta_i), \sin(4\theta_i)] \\ (V_1^D, V_2^D, V_3^D, V_4^D) &= \frac{4}{N^3}\sum_{i=1}^{N}(Z_i^3 - Z_{i-1}^3)\,[\cos(2\theta_i), \sin(2\theta_i), \cos(4\theta_i), \sin(4\theta_i)]\end{aligned} \tag{1}$$

where, $Z_i = -N/2 + i$.

The key concept for the derivation of the continuous blending constraints is to evaluate the change in lamination parameters ($\Delta V$) due to ply drops. The application of this concept is presented here for deriving the blending constraint for a single in-plane lamination parameter (Eq. (6)). A comprehensive derivation of all the remaining blending constraints (Eqs. (9) and (11)) used in this paper can be found in [**?**] .

Lets denote $V_{1(N)}^A$ and $V_{1(N-X)}^A$ the value of the first in-plane lamination parameter when the laminate has respectively $N$ and $N-X$ plies. The change in lamination parameter due to a $X$ ply

drops is denoted as $\Delta V^A_{1(N)\rightarrow(N-X)}$ and it is presented in Eq. (4).

$$V^A_{1(N)} = \frac{1}{N}\sum_{i=1}^{N}\cos(2\theta_i) \tag{2}$$

$$V^A_{1(N-X)} = \frac{1}{N-X}\sum_{i=X+1}^{N}\cos(2\theta_i) \tag{3}$$

$$\Delta V^A_{1(N)\rightarrow(N-X)} = V^A_{1(N)} - V^A_{1(N-X)} = \underbrace{\frac{1}{N}\sum_{j=1}^{X}\cos(2\theta_j)}_{\substack{\text{Term containing the}\\ \text{dropped plies}}} + \underbrace{\left(\frac{1}{N}-\frac{1}{N-X}\right)\sum_{i=1}^{N-X}\cos(2\theta_i)}_{\substack{\text{Term containing the plies}\\ \text{present in both sections}}} \tag{4}$$

where $X$ is the number of dropped plies, $N$ is the total number of plies, $\theta_j$ represent the orientation of the dropped plies and $\theta_i$ the orientation of the plies left in the stacking sequence. The maximum and minimum value of Eq. (4) occurs respectively for $[\theta_j,\theta_i] = [0°,90°]$ and for $[\theta_j,\theta_i] = [90°,0°]$ at which $\Delta V^A_{1(N)\rightarrow(N-X)}$ is:

$$\max_{(\theta_j,\theta_i)} ||\Delta V^A_{1(N)\rightarrow(N-X)}|| = 2\frac{X}{N} \tag{5}$$

This implies that no blendable solution can be found if, in two adjacent sections, the change in $V^A_1$ is greater than $2(X/N)$. By applying the same approach to the remaining in-plane lamination parameters, it can be shown that this limit holds. Thus, it is possible to define a blending constraint for single in-plane lamination parameter change as:

$$||\Delta V^A_{k(N)\rightarrow(N-X)}|| \leq 2\frac{X}{N}, \qquad \text{for } k = 1,2,3,4 \tag{6}$$

An analogous procedure can be implemented in the retrieval of a blending constraint for single out-of-plane lamination parameter, also in this case it is possible to obtain a single equation [**?**] applicable to all four out-of-plane lamination parameters separately. However, applying eight constraints on single in-plane and out-of-plane lamination parameters change between all combinations of two different sections in a structure can drastically increase the number of total constraints to take into account during optimization. In order to reduce the number of constraints, the Euclidean distance (Eq. (7)) can be used to take into account the simultaneous change of more that one lamination parameter, leading to Eq. (8) that constrains all four in-plane lamination parameters simultaneously.

$$\left(E^{IP}_{(N)\rightarrow(N-X)}\right)^2 = \sum_{k=1}^{4}\left(\Delta V^A_{k(N)\rightarrow(N-X)}\right)^2 \tag{7}$$

$$\left(E^{IP}_{(N)\rightarrow(N-X)}\right)^2 \leq 6.25(X/N)^2 \tag{8}$$

Similarly, a constraint can be derived for all four out-of-plane lamination parameters. However, since in this paper only symmetric stacking sequence with even number of plies are taken into account (Figure 2), the in-plane and out-of-plane constraints are written as in Eqs. (9). The scalar value '6.25' is calculated, like for Eq. (5), by finding the maximum of a summation of trigonometric functions representing the plies dropped and kept in the laminate [**?**] . This maximum always corresponds to stacking sequence that are unlikely to be used in aerospace application because they do not follow some of the most common used composite design guidelines [**?**] like the 10% rule. Therefore, the derived blending constraints are conservative in the sense that they are effective also when composite

design guidelines are not enforced and not conventional stacking sequence are used. Therefore, in order to tighten the constraints two coefficients $\alpha$ and $\beta$ have been added. These parameters allows the radius of the hypersphere limiting the $\Delta V$ to be reduced.

$$\begin{aligned}\left(E^{IP}_{(N)\rightarrow(N-2X)}\right)^2 &\leq \alpha\ 6.25\left(\frac{2X}{N}\right)^2 \\ \left(E^{OOP}_{(N)\rightarrow(N-2X)}\right)^2 &\leq \beta\ 6.25\left[2\left(3\left(\frac{X}{N}\right)-6\left(\frac{X}{N}\right)^2+4\left(\frac{X}{N}\right)^3\right)\right]^2\end{aligned} \tag{9}$$

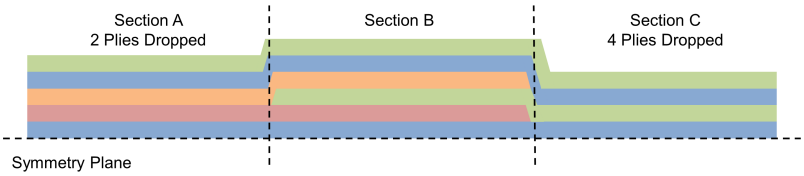


**Figure 2:** Ply-drops illustration for symmetric laminates with even number of plies.

It is also possible to combine both in-plane and out-of-plane lamination parameters change in one single blending constraint by use, one more time, of the Euclidean distance and obtaining Eq. (11).

$$\left(E^{IP,OOP}_{(N)\rightarrow(N-2X)}\right)^2 = \sum_{k=1}^{4}\left(\Delta V^{A}_{k(N)\rightarrow(N-2X)}\right)^2 + \sum_{k=1}^{4}\left(\Delta V^{D}_{k(N)\rightarrow(N-2X)}\right)^2 \tag{10}$$

$$\left(E^{IP,OOP}_{(N)\rightarrow(N-2X)}\right)^2 \leq 6.25\left[\underbrace{\alpha\left(\frac{2X}{N}\right)^2}_{\text{In-Plane}} + \underbrace{\beta\left[2\left(3\left(\frac{X}{N}\right)-6\left(\frac{X}{N}\right)^2+4\left(\frac{X}{N}\right)^3\right)\right]^2}_{\text{Out-of-Plane}}\right] \tag{11}$$

The blending constraints presented here (Eqs. (6), (9) and (11)) limit the change in lamination parameters between adjacent laminates and are function of the thickness change (or ply drops ratio $X/N$). However, optimizing at the same time thicknesses and lamination parameters while enforcing constraints that are function of both, results in a non-convex optimization problem. To overcome this issue, a the four-step strategy presented in Section 3.1 is adopted.

In order to provide the reader with a visual representation of the constraints, lets take into account the situation presented in Figure 3, where a multi-section laminate is subjected to $X$ ply drops from a section with $N$ plies to another with $N-X$ plies. Lets now reproduce this situation in the lamination parameters space for $V_1^A$ and $V_2^A$ (Figure 4). In this example the starting laminate section has $N$ equal to 20 plies and it is used to generate all possible $N-X$ plies blended sections by removing $X$ equal to 2 and 4 plies. Blending constraints for the two different ply drops are shown to be capable of including all possible $N-X$ plies blended sections.

## 3 Optimization problem

The optimization problem is carried out using a bi-step optimization strategy. First, a gradient based optimization (continuous) step optimizes the stiffness matrices of the wing sections via lamination parameters. Second, a genetic algorithm (discrete optimization) is used to retrieve a manufacturable

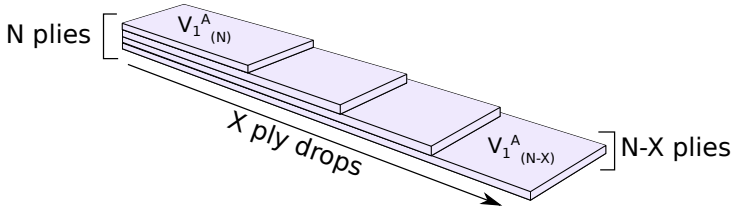


**Figure 3:** Multi-section laminate and ply-drops illustration

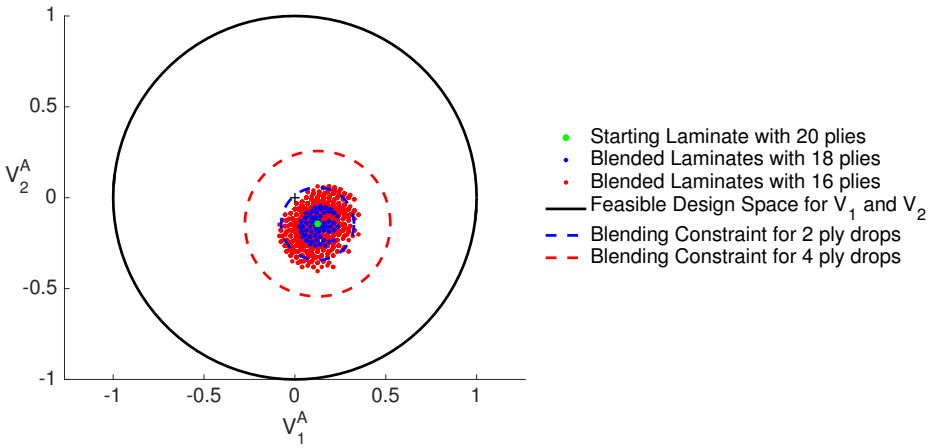


**Figure 4:** Example of a 20 plies laminate and all its possible blended laminates with 2 and 4 ply drops.

stacking sequences starting from the continuous results obtained at the first step. The two steps are described respectively in Sections 3.1 and 3.2. Section 3.3 introduce the wing model used together with the load case and the mechanical constraints.

### 3.1 Continuous optimization via NASTRAN SOL 200

The blending constraints limit the change of lamination parameters between each section as function of their change in thickness. Applying those constraints while simultaneously optimizing thickness and lamination parameters leads to a non-convex optimization problem. Therefore, the following 4-step strategy is employed (Figure 5).

For the case where blending constraints are enforced. The first step of this algorithm is the conventional convex optimization of the structure thicknesses and lamination parameters without blending constraints. This step provides a feasible starting point before the introduction of the blending constraints. The unblended design ($X_U$) is used as starting point for step 2, where blending constraints are considered. In step 3, a repair function rounds up the thicknesses of blended design ($X_B$) to an even number of plies. After the repaired design ($X_R$), lamination parameters are optimized one last time in step 4 while thicknesses are fixed. During this step, the feasibility of the structure is maximized, meaning that the objective function during this step is to maximize the reserve factors of all the mechanical constraints. Rounding of thicknesses and maximizing of reserve factors modify

the stiffness of the structure, leading to internal load redistribution. Therefore, step 2-4 are repeated until convergence to a final continuous design ($X_{FC}$). After the final continuous design is obtained, a stacking sequence retrieval GA is employed to retrieve a blended final discrete design ($X_{FD}$).

In case blending is not required, step 2 is avoided and steps 1,3-4 are repeated until convergence. The overall strategy is presented in Figure 5.

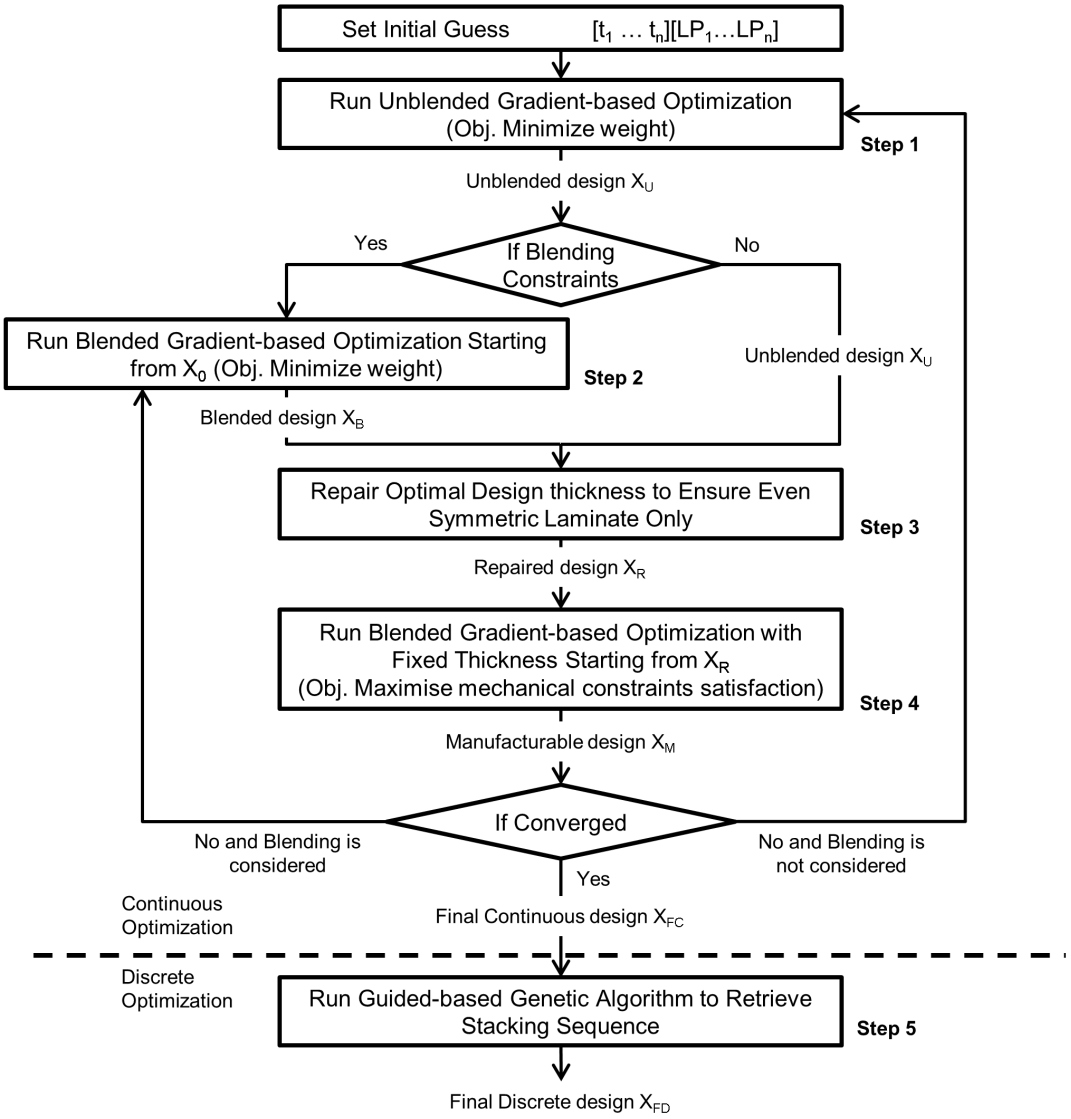


**Figure 5:** Proposed optimization strategy including blending constraints.

The optimizer and FEM solver used in this optimization is NASTRAN SOL 200, whereas the proposed strategy is implemented and run externally via Python script. NASTRAN, as well as other optimizers, allows the user to combine responses, design variables and model properties (e.g. Young modulus or stiffness module) and to define new responses that can be used during optimization. This

capability allowed an easy implementation of the blending constraints inside the optimizer. Other gradient-based optimization tools with comparable capabilities can also be used.

### 3.2 Discrete optimization via OptiBLESS

The OptiBLESS [**?**] open source stacking sequence optimization toolbox developed by the authors is used to retrieve manufacturable laminates (`https://github.com/TMacquart/OptiBLESS`). OptiBLESS uses a guide-based GA in order to retrieve blended stacking sequences matching the optimized lamination parameters achieved by the grandient-based optimizer (i.e. NASTRAN). According to the guide-based methodology [**?**], the thickest laminate is defined as the guide-laminate. Other laminates from the same structure are obtained by dropping plies from the guide-laminate therefore ensuring the final design is blended. Additionally, manufacturing design guidelines such as the ten percent rule and the disorientation guideline are enforced during the discrete optimization. The complete list of composite design guidelines can be found in the work of Irisarri et al. [**?**].

The outcome of the continuous optimization step is used as starting point for the discrete optimization. After the continuous optimization each wing section is optimized in terms of laminate thickness and lamination parameters. The thickest laminate within each substructure (i.e. skins and spars) is identified and set as the guide. Next, the ply angles describing the guide laminate stacking sequence and ply drops are used as design variables in OptiBLESS. Doing so ensure some level of structural continuity between each of the substructure laminates. That is, the plies of thinnest top skin laminate are ensured to span the entire top skin structure due to the guide-based coding implemented in OptiBLESS.

The genotype used in OptiBLESS to describe composite structures is given as:

$$Genotype = \left[ \underbrace{[\theta_1\ \theta_2\ ...\ \theta_n]}_{\text{Ply angles}} \underbrace{[\Xi_1\ \Xi_2\ ...\ \Xi_D]}_{\text{Drop off}} \right] \tag{12}$$

The guide laminate is fully defined by the $\theta$'s. Other laminates are obtained by dropping plies from the guide stacking sequence. Since the number of plies associated with each section of structure is known from the continuous optimization, the ply drop off design variables denote which ply of guide stacking sequence must be dropped. For instance, consider a structure composed of a 5-ply guide laminate and two other laminates of 4 and 2 plies each. The genotype for such structure would be :

$$Genotype = [[\theta_1\ \theta_2\ \theta_3\ \theta_4\ \theta_5][\Xi_1\ \Xi_2\ \Xi_3]] = [[\theta_1\ \theta_2\ \theta_3\ \theta_4\ \theta_5][1\ 3\ 4]] \tag{13}$$

where the guide stacking sequence is simply $[\theta_1\ \theta_2\ \theta_3\ \theta_4\ \theta_5]$ and the stacking sequence for 4 and 2 plies laminates are respectively $[\theta_2\ \theta_3\ \theta_4\ \theta_5]$ and $[\theta_2\ \theta_5]$.

The objective function used during the discrete optimization represents the lamination parameter matching quality between the continuous and discrete design. In other words, OptiBLESS is set to retrieve blended stacking sequences with lamination parameters matching the lamination parameters obtained at the end of the continuous optimization. This objective function is simply expressed as the root mean square error (RMSE) between the continuous and discrete lamination parameters as shown in Eqs. (14 and 15).

$$Fitness(\boldsymbol{\theta},\Xi) = \frac{1}{N_{lam}} \sum_{s=1}^{N_{lam}} RMSE_s(\boldsymbol{\theta},\Xi) \tag{14}$$

$$RMSE_s(\boldsymbol{\theta},\Xi) = \sqrt{\frac{1}{8} \sum_{i=1}^{8} \left(\widetilde{\mathbf{LP}}_{i,s} - \mathbf{LP}_{i,s}(\boldsymbol{\theta},\Xi)\right)^2} \tag{15}$$

where $N_{lam}$ is the total number of laminate sections in a structural component (i.e. upper wing skin), $\widetilde{\mathbf{LP}}_{i,s}$ is the vector of input parameters for section $s$ and $\mathbf{LP}_{i,s}$ is the vector of lamination parameters obtained by the GA. Stacking sequences are converted into lamination parameters in order to evaluate the fitness using the following notation:

$$\mathbf{LP} = [V_1^A\ V_2^A\ V_3^A\ V_4^A,\ V_1^D\ V_2^D\ V_3^D\ V_4^D] \tag{16}$$

According to the fitness function given in Eq. (14), the best retrieved stacking sequence would be a manufacturable stacking sequence exactly matching the optimized lamination parameters obtained by NASTRAN.

### 3.3 ONERA Wing Model

An ONERA internal wing model is used as a test case for the blending constraints. The wing model is characterized by upper and lower skins, front and rear spars, 32 ribs, 13 stringers and represent a realistic aircraft wing (e.g. A320 or B737). Wing dimensions and load case are presented in Table 1.

The wing skins and spars are divided respectively in eleven and five different sections (Figure 6), each section is optimized by means of section thickness ($t$) and eight lamination parameters ($V_1^A$, $V_2^A$, $V_3^A$, $V_4^A$, $V_1^D$, $V_2^D$, $V_3^D$, $V_4^D$). Ribs and stiffeners are made of quasi-isotropic stacking sequences but are not optimized. The aeroelastic loads are calculated via Doublet Lattice Method (DLM) inside NASTRAN SOL 144, where the aircraft is trimmed. A quasi-isotropic initial design with constant thickness along the wingspan is used as starting point for the continuous optimization.

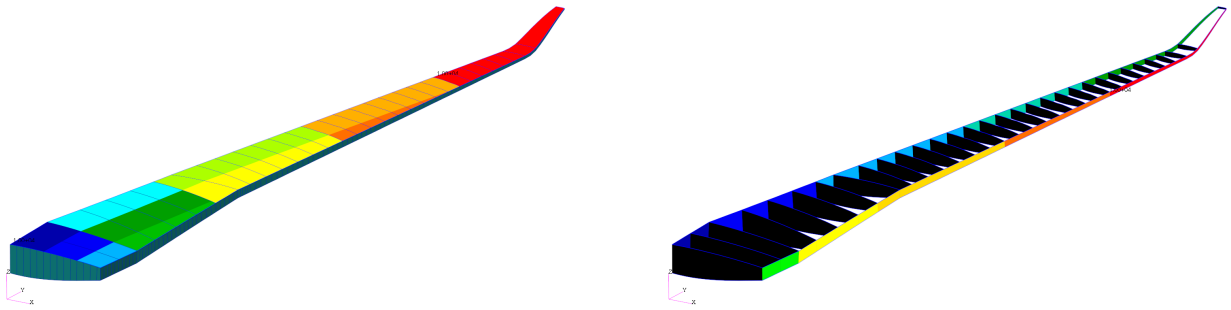

**(a)** **(b)**

**Figure 6:** (a) Sections of the upper and lower skin, and (b) sections in the front and rear spars plus ribs distribution.

A part from the bending constraints, other sets of constraints are considered during the optimization. One set of constraints is represented by the compatibility equations [**?**, **?**], these ensure that each set of in-plane and out-of-plane lamination parameters leads to a realistic A and D stiffness matrix.

**Table 1:** Wing features and load case used in the optimization.

| **Wing geometric characteristics** | |
|---|---|
| Half Wingspan | 18.5 m |
| Wing Area | 111 $m^2$ |
| Wing Dihedral | 3.5° |
| Leading edge Sweep Angle | 18° |
| **Load case data** | |
| Mach | 0.48 |
| Altitude | 0 ft |
| Weight | 26000 kg |
| Acceleration | 2.5 g |

Mechanical constraints on strength and local buckling are also used during the optimization.

The strength constraint used have been derive by IJsselmuiden et al. [**?**] and represent an analytical expressions for a conservative failure envelope based on the Tsai-Wu failure criterion in strain space. The conservative failure envelope, that is valid for any ply orientation, determine a region in strain space that guaranteed no failure would occur within a laminate, irrespective of the ply orientation angles present. A representation of such space is given in Figure 7. In order to use the envelope as a constraint an expression for laminate failure is expressed as in Eq. 17.

$$\lambda_S = \frac{b}{a} \tag{17}$$

where failure occurs for $\lambda_S < 1$, $a$ is the distance between the origin and an arbitrary point $P$ in the feasible design space, and $b$ the length of a vector from the origin to a point on the envelope boundary, $P^\star$, as shown in Figure 7.

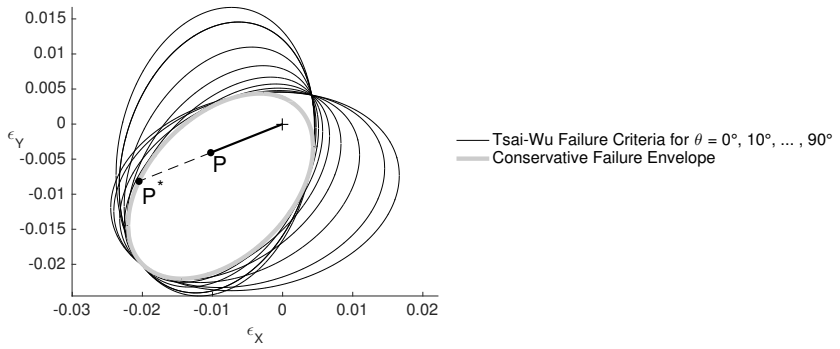


**Figure 7:** Conservative failure envelope in strain space developed by IJsselmuiden et al. [**?**] .

Local buckling is constrained via the closed formula Eq. (18) in all regions delimited by two ribs and two stiffeners and is enforced only in the wing skins.

$$\lambda_B = \pi^2 \frac{D_{11}(m/a)^4 + 2(D_{12} + 2D_{33})(m/a)^2(n/b)^2 + D_{22}(n/b)^4}{(m/a)^2 N_X + (n/b)^2 N_Y} \tag{18}$$

where buckling occurs for $\lambda_B < 1$, $N_X$ and $N_Y$ are the stresses in the longitudinal and transverse directions, $a$ and $b$ are the corresponding region dimensions and $m$ and $n$ are the corresponding number of half waves.

Constraints satisfactions for both strength and buckling are presented in Section 4 in form of failure index (Eq. (19)) where $\lambda$ is either $\lambda_S$ or $\lambda_B$ and failure occurs when FI > 1.

$$\text{FI} = \frac{1}{\lambda} \tag{19}$$

# 4 Results

This section first presents the differences between the final continuous designs obtained with and without the blending constraints. Second, the focus is set on the discrepancies between the continuous and discrete final designs and on how the blending constraints affect them. Finally, constraints satisfaction for the retrieved stacking sequence are verified to assess whereas or not the blending constraints lead to a more realistic continuous optima.

The continuous optimization performed with blending constraints are obtained with Eqs 9 and 11, where $\alpha = \beta = 0.5$.

## 4.1 Final continuous designs

The thickness distributions for the final continuous design ($X_{FC}$) obtained with and without the blending constraints are shown in Figures 8 and 9. Each figure shows the thickness in the different laminate sections for the four optimized components of the wing, namely the upper and lower wing skins and the front and rear wins spars. Major differences between the blended ($X^B_{FC}$) and unblended ($X^U_{FC}$) final continuous designs can be found in the lower skin, front and rear spars where a higher level of thickness variations is observed when blending constraints are used. In general, it is possible to observe that higher thicknesses have been obtained for the blended solution. This is true in all the components except for the upper wing skin where, in some sections, the thickness has been reduced. However, as it is shown in Figure 15b, the generic trend correspond to an increase in thickness resulting from the enforcement of blending constraints.

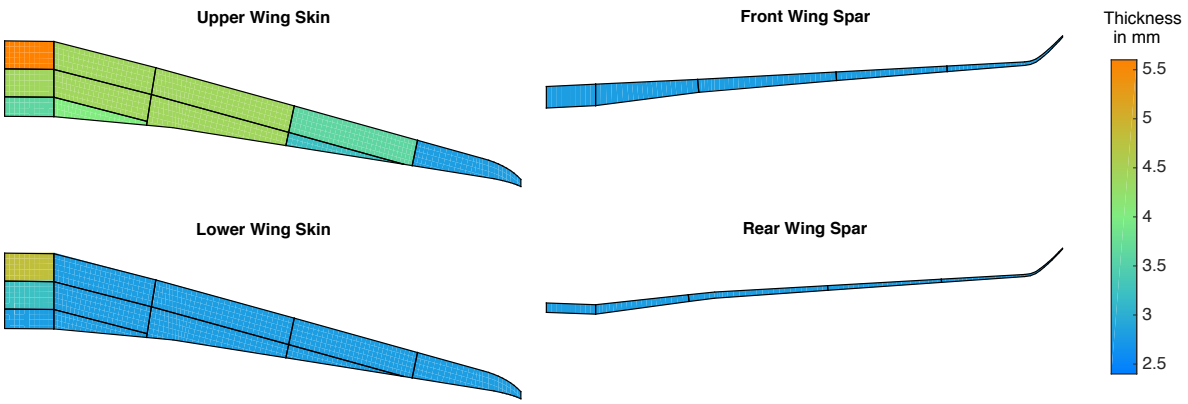


**Figure 8:** Thickness distribution for the final continuous design without blending ($X^U_{FC}$).

Differences in stiffness distributions between the blended ($X^B_{FC}$) and unblended ($X^U_{FC}$) continuous design are shown in Figures 10 and 11. This distribution is a visual representation of the $A_{11}$ element of the in-plane stiffness matrix with respect to the element coordinate system. It allows a quick interpretation of the optimized lamination parameters by providing an indication of the main fibers directions.

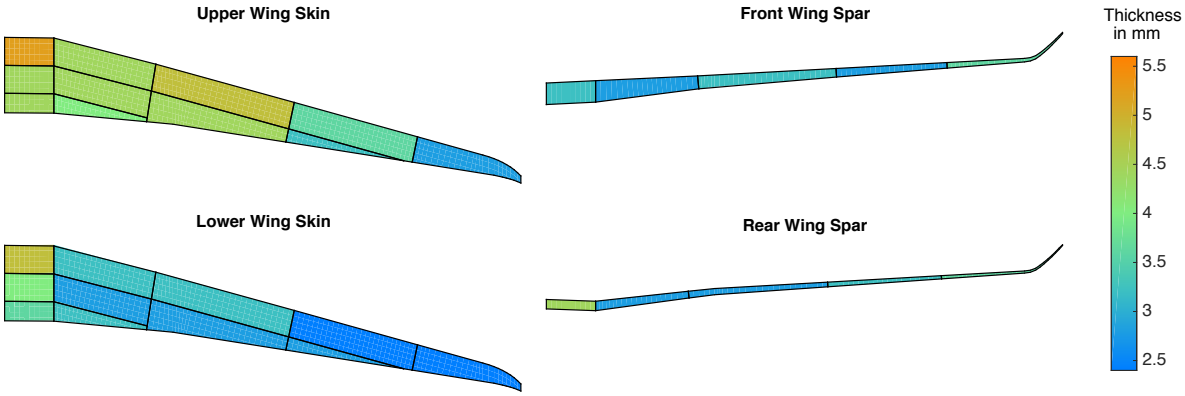


**Figure 9:** Thickness distribution for the final continuous design with blending ($X^B_{FC}$).

It is clearly visible that the unblended solution allows a greater variety of stiffness distributions and orientation. The possibility to have significantly different stiffness orientations in adjacent sections allows a better local optimization of the structure but consequently results in structural discontinuity. On the contrary, the use of blending constraints results in a smooth change of stiffness distributions along the wing span. This reduction in stiffness tailoring leads to less performing continuous optima but helps reducing structural discontinuities.

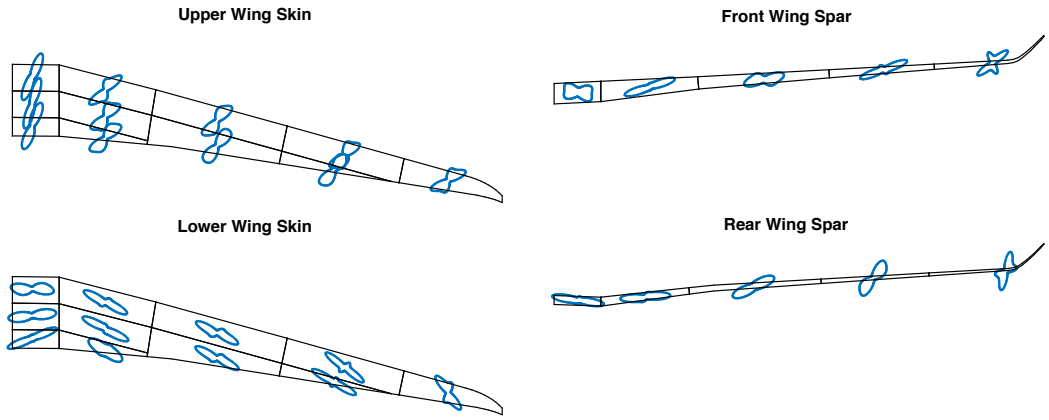


**Figure 10:** Stiffness directions for the final continuous design without blending ($X^U_{FC}$).

Mechanical constraints satisfaction is shown in Figures 12 - 14 for the blended and unblended continuous designs where constraints are violated above the value 1. While Figures 12 and 13 show the strength failure index for the four structural components, Figure 14 shows the buckling failure index for the upper wing skins only. Buckling for the lower wing skin is not shown since no buckling occurs in that component and no buckling has been considered during the optimization of the front and rear spars. The use of Eq. (18) limit the buckling calculations to rectangular plates, therefore triangular regions have not been taken into account and are not present in Figure 14. For both designs the continuous optimization obtained feasible solution where none of the constraints have been violated, proving that the effectiveness of the multistep optimization strategy proposed in Section 3.1.

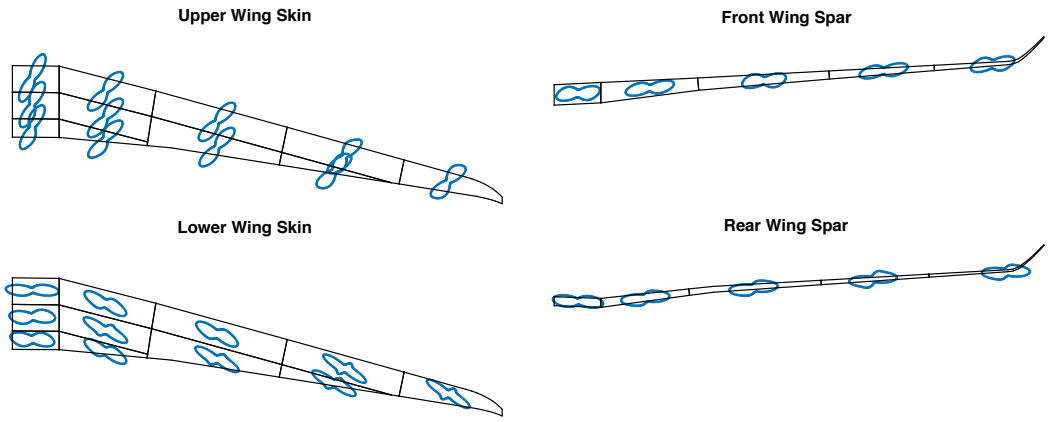


**Figure 11:** Stiffness directions for the final continuous design with blending ($X^B_{FC}$).

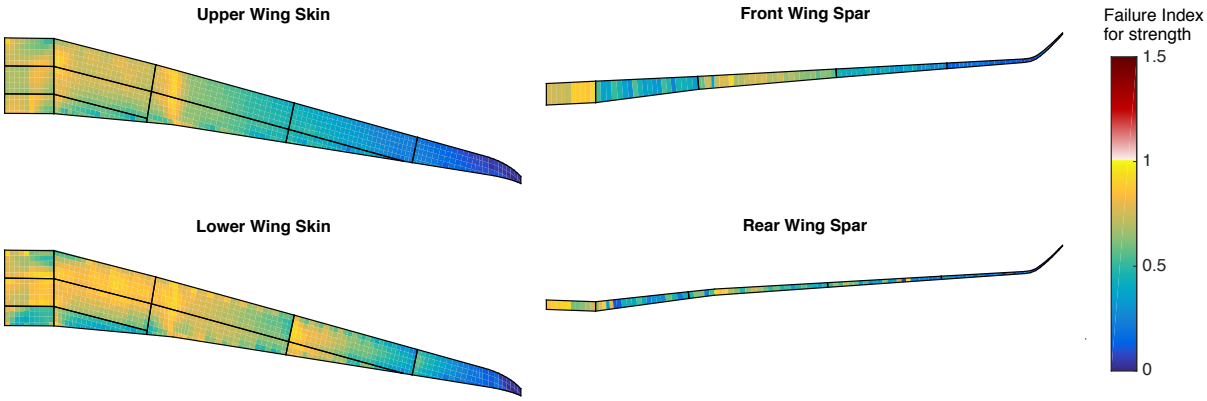


**Figure 12:** Strength constraint for final continuous design without blending ($X^U_{FC}$).

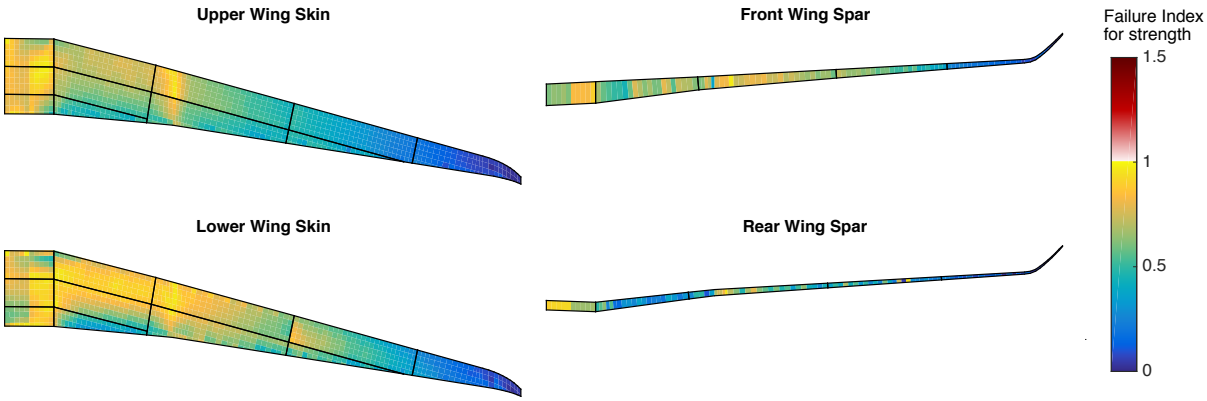


**Figure 13:** Strength constraint for final continuous design with blending ($X^B_{FC}$).

## 4.2 Final discrete designs

One of the main disadvantages in using bi-step approaches, is that there no guarantee to retrieve a discrete solution that perfectly matches the continuous optima. This leads to less realistic continuous

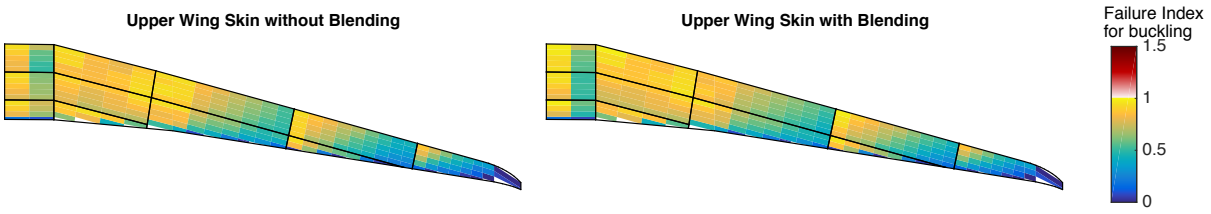


**Figure 14:** Buckling constraint in the upper wing skins for the final continuous design without ($X^U_{FC}$) and with blending ($X^B_{FC}$).

optima and significant discrepancies between continuous ($X_{FC}$) and discrete ($X_{FD}$) designs. By adding blending constraints in the continuous optimization step, the above mentioned discrepancies can be reduced and more realistic continuous optimum can be found. This is shown in Figure 15a where the root mean square error (RMSE), used by OptiBLESS to retrieve a blended stacking sequence, is presented for each structural component. RMSE between continuous and discrete designs are significantly reduced ($-59.2\%$) when the blending constraints are used in the continuous optimization. However, this result come at the price of a slightly heavier design ($+2.2\%$). This increase in weight is due to the fact that, in order to allow a smooth transition of stiffness distribution along the wing sections, the blending constraints are in fact reducing the design variable space and therefore limiting the range of available lamination parameters.


**Figure 15:** (a) RMSE in retrieving a blended structure, and (b) weight of the wing structure.

### 4.3 Constraints satisfaction after stacking sequence retrieval

Finally, we investigate the indices corresponding to mechanical failure after the stacking sequences are retrieved (Step 5 in Figure 5) in Figures 16 - 18. As one can observe, both the final discrete design with ($X^B_{FD}$) and without ($X^U_{FD}$) blending constraints do not satisfy all strength and buckling constraints. This emphasize the intrinsic difficulty of bi-step approaches in perfectly matching the discrete and continuous designs. However, the blending constraints clearly lead to a more realistic continuous optima, smaller failed areas with smaller failure indices have been achieved when the blending constraints were used. In particular, as shown in Table 2, the maximum strength constraints violations in the critical lower wing section is shown to be reduced by 47.1% due to the application of the blending constraints.

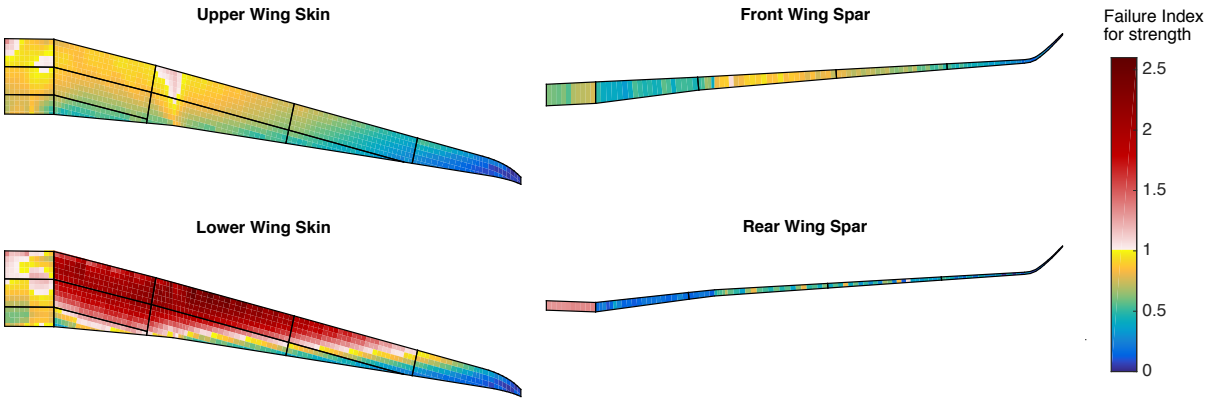


**Figure 16:** Strength constraint for final discrete design without blending ($X^U_{FD}$).

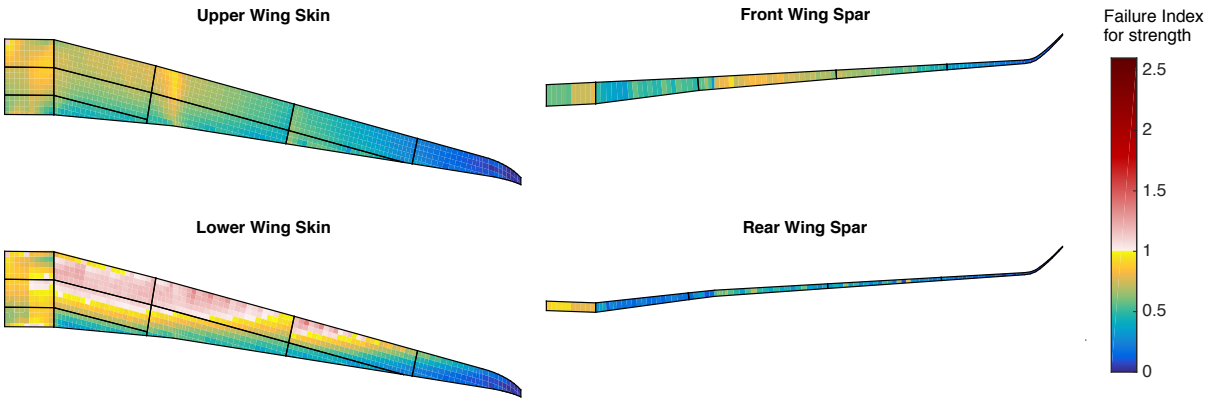


**Figure 17:** Strength constraint for final discrete design with blending ($X^B_{FD}$).

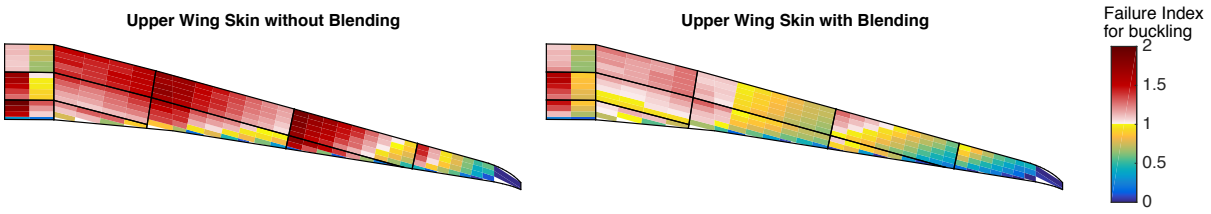


**Figure 18:** Buckling constraint in the upper wing skins for the final discrete design without ($X^U_{FD}$) and with blending ($X^B_{FD}$).

**Table 2:** Maximum failure index for the retrieved stacking sequence.

| | **Strength** | **Buckling** |
|---|---|---|
| **Without blending constraints** | 2.595 | 1.922 |
| **With blending constraints** | 1.373 | 1.572 |
| **Reduction in maximum failure index violation due to blending constraints** | 47.1% | 18.2% |

# 5 Conclusion

Locally optimized composite structures are likely to lead to optimum designs that are affected by structural discontinuities between adjacent regions. One possibility to minimize those discontinuities and to ensure structural integrity is to enforce ply continuity (i.e. blending) during the optimization throughout the whole structure. Several bi-step strategies, relying on a continuous gradient-based optimization of lamination parameters followed by a discrete stacking sequence optimization step during which blending is enforced, have been successfully used to retrieve blended solutions. However, due to the discrepancies between the two design spaces, significant differences could be observed between the continuous and discrete designs.

In the present paper a set of continuous blending constraints, recently proposed by the authors, have been applied to a bi-step approach during the aeroelastic optimization of a variable stiffness wing. Both in-plane and out-of-plane composite stiffness matrices have been optimized via lamination parameters with respect to strength (based on strain) and local buckling constraints. The continuous blending constraints have significantly reduced the discrepancies between the continuous and discrete optimum (−59.2%) by modifying the thickness distribution over the wingspan and by smoothing the change in stiffness distribution and orientation. As a result, the retrieved blended stacking sequences match more closely the continuous design a the price of at slightly heavier design (+2.2%).

Constraints satisfaction, of the retrieved stacking sequence obtained with and without the continuous blending constraints, have shown a reduction of failed elements and sections when blending constraints have been used. Moreover, failure indices violation resulted in up to 47.1% reduction when the blending constraints have been used. Although both discrete designs presented failure indices violations, due to the intrinsic discrepancies between the continuous and discrete design space, these results demonstrate that more realistic continuous designs can be obtained with the continuous blending constraints.

## 6 Acknowledgements

The research leading to these results has received funding from the European Union Seventh Framework Programme FP7-PEOPLE-2012-ITN under grant agreement n° 316394, Aerospace Multidisciplinarity-Enabling DEsign Optimization (AMEDEO) Marie Curie Initial Training Network.

## References

[1] Dillinger, J. K. S., *Static Aeroelastic Optimization of Compisite Wing with Variable Stiffness Laminates*, Ph.D. thesis, Delft University of Technology, 2014.

[2] IJsselmuiden, S. T., Abdalla, M. M., Seresta, O., and GÃijrdal, Z., "Multi-step blended stacking sequence design of panel assemblies with buckling constraints," *Composites Part B: Engineering*, Vol. 40, No. 4, 2009, pp. 329 – 336.

[3] Adams, D. B., Watson, L. T., GÃijrdal, Z., and Anderson-Coo, C. M., "Genetic algorithm optimization and blending of composite laminates by locally reducing laminate thickness," *Advances in Engineering Software*, Vol. 35(1):35-43, 2004.

[4] Campen, J. V., Seresta, O., Abdalla, M. M., and Gurdal, Z., "General blending definitions for stacking sequence design of composite laminate structure," 49th AIAA/ASME/ASCE/AHS/ASC structures, structural dynamics, and materials, 2008, pp. 7–10.

[5] Irisarri, F.-X., Lasseigne, A., Leroy, F.-H., and Riche, R. L., "Optimal design of laminated composite structures with ply drops using stacking sequence tables," *Composite Structures*, Vol. 107, 2014, pp. 559 – 569.

[6] Peeters, D. M., Hesse, S., and Abdalla, M. M., "Stacking sequence optimisation of variable stiffness laminates with manufacturing constraints," *Composite Structures*, Vol. 125, 2015, pp. 596 – 604.

[7] Dillinger, J. K. S., Klimmek, T., Abdalla, M. M., and Gurdal, Z., "Stiffness Optimization of Composite Wings with Aeroelastic Constraints," *Journal of Aircraft*, Vol. 50, No. 4, 2013, pp. 1159–1168.

[8] Liu, D., Toropov, V. V., Querin, O. M., and Barton, D. C., "Bilevel Optimization of Blended Composite Wing Panels," *Journal of Aircraft*, Vol. 48, No. 1, 2011.

[9] Macquart, T., Bordogna, M. T., Lancelot, P., and Breuker, R. D., "Derivation and application of blending constraints in lamination parameter space for composite optimisation," *Composite Structures*, Vol. 135, 2016, pp. 224 – 235.

[10] Soremekun, G., GÃijrdal, Z., Kassapoglou, C., and Toni, D., "Stacking sequence blending of multiple composite laminates using genetic algorithms," *Composite Structures*, Vol. 56, No. 1, 2002, pp. 53 – 62.

[11] Macquart, T., Werter, N., and Breuker, R. D., "Aeroelastic Tailoring of Blended Composite Structures using Lamination Parameters," 57th AIAA/ASCE/AHS/ASC Structures, Structural Dynamics, and Materials Conference, AIAA SciTech, 2016.

[12] Tsai, S. W. and Hahn, H. T., *Introduction to composite materials*, Technomic Publishing Co, 1980.

[13] *COMPOSITE MATERIALS HANDBOOK VOLUME 3. POLYMER MATRIX COMPOSITES MATERIALS USAGE, DESIGN, AND ANALYSIS*, 2002.

[14] *Optibless - an open-source toolbox for the optimisation of blended stacking sequences (accepted). In The seventeenth European Conference on Composite Materials (ECCM17)*, 2016.

[15] Fukunaga, H. and Sekine, H., "Stiffness design method of symmetric laminates using lamination parameters," *AIAA Journal*, Vol. 30, No. 11, 1992, pp. 2791–2793.

[16] Raju, G., Wu, Z., and Weaver, P., "On Further Developments of Feasible Region of Lamination Parameters for Symmetric Composite Laminates," *55th AIAA/ASME/ASCE/AHS/ASC Structures, Structural Dynamics, and Materials Conference, AIAA SciTech, (AIAA 2014-1374)*, 2014.

[17] Ijsselmuiden, S. T., Abdalla, M. M., and GÃijrdal, Z., "Implementation of Strength-Based Failure Criteria in the Lamination Parameter Design Space," *AIAA Journal*, Vol. 46, No. 7, 2008, pp. 1826–1834.